Journal Name

ARTICLE TYPE

Cite this: DOI: 10.1039/xxxxxxxxxx

Received Date
Accepted Date

DOI: 10.1039/xxxxxxxxxx

www.rsc.org/journalname

Titanium deposition from ionic liquids - proper choice of electrolyte and precursor

Claudia A. Berger,[a] Maria Arkhipova,[b] Attila Farkas,[a] Gerhard Maas,[b] and Timo Jacob[a,c]

In this study titanium isopropoxide was dissolved in 1-butyl-3-methyl-imidazolium bis(trifluoromethylsulfonyl)imide (BMITFSI) and further in a custom-made guanidinium-based ionic liquid ($N_{11}N_{11}N_{pip}$GuaTFSI). Electrochemical investigations were carried out by means of cyclic voltammetry (CV) and the initial stages of metal deposition were followed by *in-situ* scanning tunneling microscopy (STM). For BMITFSI we found one large cathodic reduction peak at a potential of –1.2 V *vs.* Pt, corresponding to the growth of monoatomic high islands. The obtained deposit was identified as elemental titanium by Auger Electron Spectroscopy (AES). Further, we found a corresponding anodic peak at –0.3 V *vs.* Pt, which is associated with the dissolution of the islands. This observation leads to the assumption that titanium deposition from the imidazolium-based room-temperature ionic liquid (RTIL) proceeds in a one-step electron transfer. In contrast, for the guanidinium-based RTIL we found several peaks during titanium reduction and oxidation, which indicates a multi-steps electron transfer in this alternative electrolyte.

1 Introduction

One of the most prominent features of elemental titanium is the ability to passivate during air contact, by forming an oxidic layer, which protects the underlying metal from corrosion. Further, it exhibits high mechanical strength, low density and high thermoconductivity. Hence, titanium coatings have a wide range of applications in chemical industry, aerospace engineering, shipbuilding, automobile industry and in medical engineering, as well, attributable to excellent compatibility with bodily tissue.

The conventional industrial method to receive titanium coatings via high temperature meltings requires large amounts of energy and titanium salts[1], a process that is not suitable and economically too expensive. Therefore, electrochemical deposition of titanium from non-aqueous solvents seems to be the future of titanium coatings. However, according to Biallozor and Lisowska[2,3] past attemps to use common organic solvents as a medium for titanium deposition have not been successful. Here, one alternative is to use ionic liquids as electrolyte to realize electrochemical deposition.

Room-temperature ionic liquids (RTILs) are organic salts, which are in molten state at room-temperature and consist solely of ions[4]. Here, many combinations of different anions and cations are possible, which results in a large variety of different RTILs with tunable physicochemical properties tailored for specific applications[5]. Besides well-investigated ILs with imidazolium, pyridinium or piperidinium cations for example, new types of ILs are also consistently developed. Here, one example are hexaalkyl-substituted guanidinium cations, where all six alkyl groups can be modified separately, allowing for an active tuning of the IL properties[6].

In general, RTILs posses remarkable features such as extremely wide electrochemical windows and high ionic conductivities in combination with low vapour pressure and high thermal stability[7–12]. There are also unfavourable properties such as relatively high viscosities and high synthesis costs. Further, possible toxicities and ecologically damaging impacts are not yet fully estimated. Nevertheless, RTILs provide access to the electrodeposition of unnoble metals, which can not be deposited from aqueous solutions.

There have already been several attempts to deposit elemental titanium from its halides in various ionic liquid electrolytes, but so far with only minor success. Instead of pure titanium layers mostly titanium subhalides[13] or in the best cases Ti-Au-surface-alloys[14–16] were obtained. One reason for this could be the complex electrochemical behaviour of titanium salts in solution, as numerous studies in various electrolytes have revealed[15,17–21].

In the present work we show the successful electrochemical deposition of elemental titanium layers from its propoxide in an imidazolium-based as well as in a custom-made guanidinium-based ionic liquid.

[a] Institute of Electrochemistry, Ulm University, Alber-Einstein-Allee 47, 89081 Ulm, Germany; Email: Timo.Jacob@uni-ulm.de
[b] Institute of Organic Chemistry I, Ulm University, Ulm, Germany.
[c] Helmholtz-Institute-Ulm (HIU), Ulm, Germany.

2 Results and discussion

2.1 Cyclic voltammetry

Figure 1 shows the first cycle of the cyclic voltammogramms of pure BMITFSI (dashed line) and with addition of 0.1 mol·l^{-1} Ti(O^{i}Pr)$_4$ (solid line) on Au(111), recorded with a scan rate of 50 mV/s. The CV of pure BMITFSI shows a broad double-layer-type behaviour over a potential range of 4 V. The potential where the irreversible decomposition of the electrolyte takes place lies outside this potential range, remarkably occuring with low current densities around the reversal potentials in the CV. After adding 0.1 mol·l^{-1} Ti(O^{i}Pr)$_4$, one can observe a single broad cathodic hump C$_1$ at –1.2 V *vs.* Pt. This CV leads to the assumption that titanium deposition from Ti(O^iPr)$_4$ in BMITFSI possibly proceeds via a one-step process, whereby the dissolved titanium(IV) salt is directly reduced to elemental titanium(0) by a single four-electron transfer. This is in contrast to recent studies [13], where no reduction peak could be observed for the solution of Ti-isopropoxide in a phosphonium-based IL. The corresponding charge of about 2 mC/cm^2 as derived from the CV (see Fig. 1) is equivalent to the overall deposition of around ten layers of titanium. The occuring broad anodic peak A$_1$ is caused by the titanium oxidation and the cathodic peak C$_1$ as corresponding potential window opening experiments revealed. The charge determined for the A$_1$ peak amounts to 1 mC/cm^2, which leads to the assumption that these processes are either not fully reversible, or the dissolved titanium possesses a lower oxidation state than in the originally dissolved titanium salt. The inset in Fig. 1 shows the CV of the system Ti(O^{i}Pr)$_4$/BMITFSI recorded with a scan rate of 5 mV/s. Here, it is noticeable that cathodic peak C$_1$ splits up and an additional shoulder at –800 mV becomes visible. This could be an indication for a titanium underpoten-tial deposition (UPD), which is in good accordance with previous studies of Freyland *et al.* [14]. The derived charge from this cathodic peak amounts to 15 mC/cm^{-2}, which corresponds to a titanium deposition of around 20 layers. Here, the related anodic charge is also somewhat lesser (10 mC//cm^{-2}) what confirm the assumption of irreversible processes towards titanium at these scan rates.

Figure 2 shows the first cycle of the cyclic voltammogramms for pure N$_{11}$N$_{11}$N$_{pip}$Gua TFSI on Au(111) (dashed line) and with 0.1 mol·l^{-1} Ti(O^{i}Pr)$_4$ added (solid line) recorded with a scan rate of 50 mV/s. The CV obtained for the pure guanidinium-based IL shows also a flat double-layer-type behaviour over a potential range of 4 V. After addition of the titanium salt, several cathodic and anodic peaks appear. This leads to the assumption that the reduction, respectively oxidation, of titanium in this IL proceeds through a number of intermediate stages, in marked contrast to BMITFSI (Fig. 1). It is noticeable that there is a cathodic peak at around –1 V in Fig. 2, which is at a similar potential as C$_1$ in Fig. 1. However, the value of the correlated current density is much lower for the guanidinium-based IL, which supports the assumption of several intermediates in the reduction process. The charge derived from peak C$_1$ in Fig. 2 amounts to 150 nC/cm^2. The charge of peak C* in Fig. 2 is of the same order. The sum of the charges of these two peaks complies with a titanium deposition of around 5×10^{11} atoms per cm^2. In comparison to the CV in Fig. 1, one can also notice an oxidation peak A$_1$ at a potential of 0.1 V, which means a similar potential in both CVs. By integration of the anodic peaks between potentials of 0 to 1 V one obtains a charge similar to those corresponding to peaks A$_1$ plus A*. So there are obvious differences in the deposition behavior of titanium from these two different ILs. Since the applied RTILs possess the same type of anion, the differing cations seem to influence the reduction of titanium, due to their adsorption on the working electrode surface at negative potentials. The role of cations during the metal deposition process is a well-known phenomenon and has also been reported for the deposition of aluminium and tantalum from various RTILs by Endres *et al.* [22]. The inset in Fig 2 shows the CV of Ti(O^{i}Pr)$_4$/N$_{11}$N$_{11}$N$_{pip}$GuaTFSI with a scan rate of 5 mV/s. Here the slower scan rate seems to have no significant influence on the shape of the CV. The sum of the charges of C$_1$ and C* is comparable to the CV with a scan rate of 50 mV/s, therefore we will not go in detail here separately.

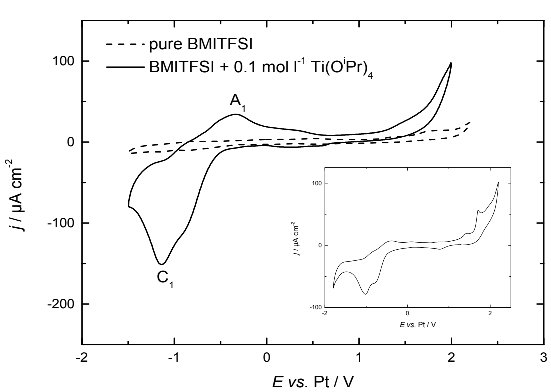

Fig. 1 CV of BMITFSI (dashed line) and BMITFSI + 0.1 mol·l^{-1} Ti(O^{i}Pr)$_4$ (solid line) on Au(111) at a scan rate of 50 mV/s. Inset: Ti(O^{i}Pr)$_4$/BMITFSI at 5 mV/s scan rate.

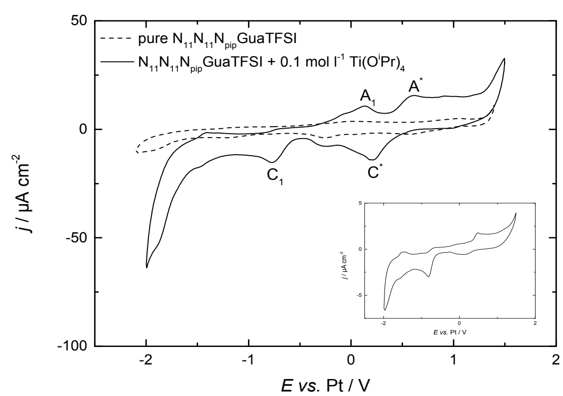

Fig. 2 CV of N$_{11}$N$_{11}$N$_{pip}$GuaTFSI (dashed line) and N$_{11}$N$_{11}$N$_{pip}$GuaTFSI + 0.1 mol·l^{-1} Ti(O^{i}Pr)$_4$ (solid line) on Au(111) at a scan rate of 50 mV/s. Inset: Ti(O^{i}Pr)$_4$/N$_{11}$N$_{11}$N$_{pip}$GuaTFSI at 5 mV/s.

2.2 *In-situ* Scanning Tunneling Microscopy

After the CV measurements structural information was obtained for titanium isopropoxide in BMITFSI using *in-situ* scanning tunneling microscopy. First, it should be mentioned that titanium isopropoxide is very sensitive to moisture, *i.e.* the presence of only traces of water leads to the formation of hardly soluble and large titanium dioxide particles, which compromises the STM investigations, making the STM imaging of these systems a formidable task. The STM image shown in Fig. 3(a) shows the free Au surface with several step edges of monoatomic height at –100 mV *vs.* Pt, which corresponds to a potential more positive than peak C_1 in the CV. Figure 3(b) has been recorded in the potential region of peak C_1 of the related CV (Fig. 1), which means –0.8 V *vs.* Pt. Here the beginning of the growth of titanium islands on the Au terraces can be observed, resulting in a Au surface that is around 26% covered with islands. After waiting for 15 minutes, Fig. 3(c) was recorded, where one can notice the proceeding growth of these islands, now covering 48% of the surface area.

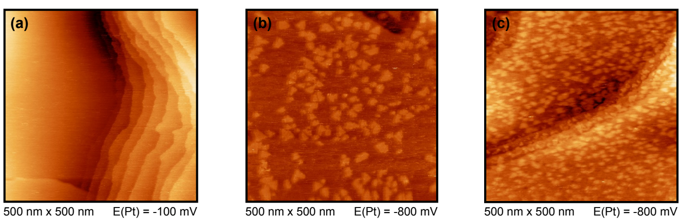

Fig. 3 *In-situ* STM images of $Ti(O^iPr)_4$/BMITFSI on Au(111) at (a) –100 mV, (b) –800 mV and (c) after 15 min at –800 mV.

The height profile corresponding to this island formation is shown in Fig. 4, where the heights of a single Au step-edge and several islands are given. Here, the height of the Au step-edge amounts to 250 pm approximately, whereas the height of the formed islands is somewhat lower, averaging to 200-250 pm. This height is in good accordance with a possible titanium deposit[14].

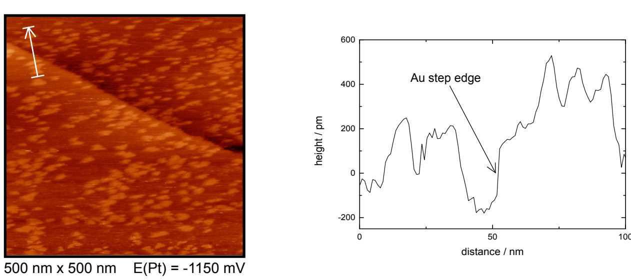

Fig. 4 *In-situ* STM image of $Ti(O^iPr)_4$/BMITFSI on Au(111) at –1150 mV with related height profile.

After further decrease of the potential to –1.5 V, the STM image in Fig. 5(a) was recorded. It shows the three-dimensional growth of titanium particles besides an almost closed monolayer. This observation encourages the assumption that there is first a Ti underpotential deposition (UPD), which passes to the Ti bulk deposition after a minimal potential decrease. This observation is in relatively good accordance with former studies by Freyland *et al.*, although there are differences in the precursor[14].

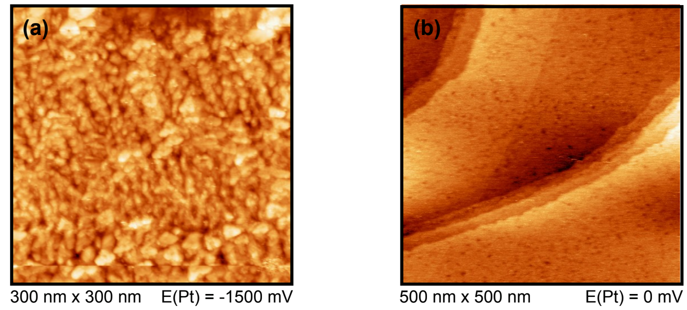

Fig. 5 *In-situ* STM images of $Ti(O^iPr)_4$/BMITFSI on Au(111) at (a) –1500 mV and (b) 0 mV.

After increasing the potential to values around 0 V and waiting for some minutes, dissolution of the islands was observed (Fig. 5(b)). After dissolution, the Au(111) surface shows small circular holes with uniform distribution over the whole substrate surface. This is in marked contrast to the pristine Au surface before titanium deposition, which is shown in Fig. 3(a). According to literature, these holes could be an indication for the formation of a Ti-Au surface alloy[14].

2.3 Auger electron spectroscopy

In order to identify the obtained deposit, its nature was investigated by Auger Electron Spectroscopy (AES). Since transfer of the sample from the electrochemical cell to the AES entails loss of the potential control, such that the microscopic state of the surface during AES measurement can not be directly assigned to one of the well-defined microscopic states observed under potential control during CV. The sole purpose of the AES measurement is to ascertain the presence of titanium deposits on the surface and further, to gain information about their oxidation state.

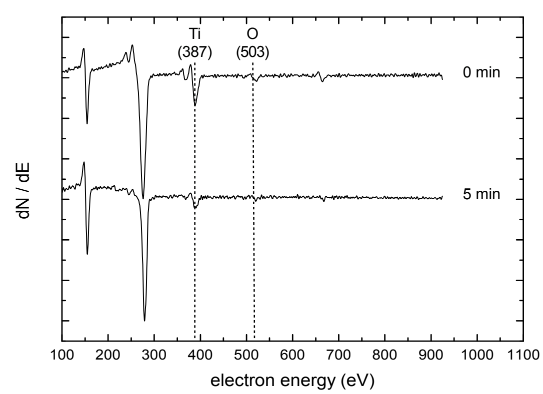

Fig. 6 Evolution of Auger electron spectra with sputter time for $Ti(O^iPr)_4$/BMITFSI on Au(111).

Figure 6 shows the obtained spectra after titanium deposition from $Ti(O^iPr)_4$/ BMITFSI on Au(111). These spectra are recorded directly and after 5 min of sputtering with an argon ion gun, in order to remove the outermost layers of titanium, which we expect to be oxidized due to remaining, not removable traces of water either in the glove box atmosphere or in the dried acetone, used for rinsing the sample to roughly remove excessive electrolyte.

This assumption is confirmed by the spectrum shown in Fig. 6 (top). It shows major titanium peaks at a binding energy of 387 eV (LMM) and a major oxygen peak at 503 eV (KVV). This is in general agreement with literature [23]. It is not surprising to detect oxygen and titanium, since elemental titanium is very sensitive to traces of water. The spectrum also shows the presence of fluorine (659 eV), sulfur (153 eV) and carbon (275 eV) from the resid-ual ionic liquid since a thin layer of electrolyte has been left on the surface to protect the deposited titanium layer. These peaks are not considered for the present investigation. The spectrum of the sample after sputtering is also shown in Fig. 6 (bottom). Here, one can notice that there is titanium (387 eV) present on the electrode surface, while the oxygen signal has completely dis-appeared. This shows that indeed elemental titanium has been deposited, since the lower metal layers are not oxidized. So the upper layers which consist of titanium dioxide have to be formed after the deposition process, otherwise all titanium layers would have been oxidized *ab initio*.

3 Conclusions

In this work we have studied the electrochemical deposition of elemental titanium from titanium isopropoxide in RTILs on Au(111) model electrodes. By combining CV, *in-situ* STM and Auger electron spectroscopy, we could show that using specific RTILs elemental titanium can be deposited on the electrode. Further, we observed that the electrochemical behaviour of the titanium system seems to be influenced by the cations of the applied electrolyte. According to our CV and STM investigations, the imidazolium-based IL showed the titanium UPD passing over to the OPD, but no former reduction steps of the titanium salt in solution. So we suggest a four-electron transfer in a single step during reduction of Ti(IV) to Ti(0) for this system. Using Auger electron spectroscopy we could further confirm that the lower lying layers of the deposit are indeed elemental titanium. In constrast, the CV of the guanidinium-based IL shows a multiple-step reduction, respectively oxidation, of the titanium salt. Two major peaks could be observed, which seem to be related to the titanium reduction/oxidation. This leads to the assumption that Ti(IV) is first reduced in solution at relatively positive potentials and in a further reduction step at negative potentials elemental titanium seems to be deposited, however in relatively small amounts according to the charges derived from the CV (<1 ML).

4 Experimental

1-Butyl-3-methylimidazolium bis(trifluoromethylsulfonyl)imide (BMITFSI) was purchased from Merck (Merck KGaA, purity $\geq$ 99.5 %, water $\leq$ 100 ppm, halides $\leq$ 100 ppm). Additionally, various guanidinium-based ionic liquids (Fig. 7) were synthesized and examined towards their suitability for the titanium deposition. Details of the synthesis and characterisation of the applied guanidinium-based ILs are given elsewhere [6,24,25].

Dependent on the physicochemical properties (*e.g.* electrochemical window, viscosity, moisture sensitivity, solubility of titanium salts) $N_{11}N_{11}N_{pip}$GuaTFSI was chosen as an appropriate

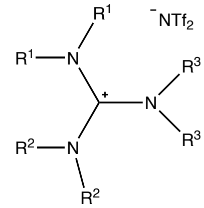

Fig. 7 Structure of $N_{11}N_{11}N_{pip}$GuaTFSI.

electrolyte for the titanium deposition. The ionic liquids were vacuum-dried for 24 h at elevated temperatures (80 ◦C) before adding the precursor titanium isopropoxide (99.995% $Ti(O^iPr)_4$, Alfa Aesar) in a concentration of 0.1 mol·l^{-1} for the metal deposition. Despite several studies that claim titanium halides and propoxides not being ideally suited for the electrodeposition of titanium layers [13,14,16], we decided to study the properties of $Ti(O^iPr)_4$ as a precursor for the metal deposition in more detail. All experiments, including handling and storage of the used substances, were performed inside a glove box under argon atmosphere. Electrochemical investigations were carried out in self-designed cells made of KelF, each with a volume of 150 μl, and an Au(111) single crystal (MaTeck GmbH, Jülich, FRG) with 12 mm diameter acting as working electrode. As counter and *quasi*-reference electrodes Pt wires (MaTeck GmbH, Jülich, FRG) were used; thus, all potentials are given against the Pt reference. Prior to the measurements all electrodes were annealed in a hydrogen flame and cooled down slowly in an argon stream.

All CVs were recorded with a Zahner IM6 potentiostat from Zahner Elektrik controlled by the Thales Z 1.20 USB software. Electrochemical *in-situ* STM studies were performed with a Digital Instruments Nanoscope 3 STM. For the preparation of the STM tips, Pt/Ir wires (80:20) were electrochemically etched in 3.5 M aqueous NaCN and coated with BASF electrophoretic paint (ZQ84-3225) to reduce the faradaic current. All images were recorded in the constant-current mode with a tip current between 1–3 nA.

Before each Auger analysis, the samples were prepared in the glovebox under argon atmosphere. After successful titanium deposition, according to the CV, the samples were rinsed with dry acetone to remove excessive electrolyte. However, a thin layer of electrolyte has been left on the electrode surface to protect the deposited titanium layers. Afterwards, the samples were transferred directly to the AES chamber using a sealed transfer vessel to avoid air contact. Auger measurements were performed with a Perkin Elmer Phi 660 AES. The analysis was done at 10 keV/22 nA. The AES depth profile was obtained by using argon ion sputtering (3 keV/1 μA).

References

1 D. Inman and S. White, *J. Appl. Electrochem.*, 1978, **8**, 375–390.

2 S. Biallozor and A. Lisowska, *Electrochim. Acta*, 1980, **25**, 1209 – 1214.

3 A. Lisowska and S. Biallozor, *Electrochim. Acta*, 1982, **27**, 105 – 110.

4 K. R. Seddon, *J. Chem. Technol. Biotechnol.*, 1997, **68**, 351–356.

5 H. Tokuda, K. Hayamizu, K. Ishii, M. A. Bin Hasan Susan and M. Watanabe, *J. Phys. Chem. B*, 2005, **109**, 6103–6110.

6 H. Kunkel and G. Maas, *Eur. J. Org. Chem.*, 2007, **2007**, 3746–3757.

7 F. Endres, *ChemPhysChem*, 2002, **3**, 144–154.

8 R. D. Rogers and K. R. Seddon, *Science*, 2003, **302**, 792–793.

9 M. J. Earle, J. M. S. S. Esperanca, M. A. Gilea, J. N. Canongia Lopes, L. P. N. Rebelo, J. W. Magee, K. R. Seddon and J. A. Widegren, *Nature*, 2006, **439**, 831–834.

10 F. Endres and S. Zein El Abedin, *Phys. Chem. Chem. Phys.*, 2006, **8**, 2101–2116.

11 F. Endres, D. MacFarlane and A. Abbott, *Electrodeposition from Ionic Liquids*, WILEY-VCH, 2008.

12 M. Freemantle, *An introduction to Ionic Liquids*, RSC Publishing, 2009.

13 F. Endres, S. Zein El Abedin, A. Y. Saad, E. M. Moustafa, N. Borissenko, W. E. Price, G. G. Wallace, D. R. MacFarlane, P. J. Newman and A. Bund, *Phys. Chem. Chem. Phys.*, 2008, **10**, 2189–2199.

14 I. Mukhopadhyay, C. Aravinda, D. Borissov and W. Freyland, *Electrochim. Acta*, 2005, **50**, 1275 – 1281.

15 T. Tsuda, C. L. Hussey, G. R. Stafford and J. E. Bonevich, *J. Electrochem. Soc.*, 2003, **150**, C234–C243.

16 J. Ding, J. Wu, D. R. MacFarlane, W. E. Price and G. Wallace, *Phys. Chem. Chem. Phys.*, 2008, **10**, 5863–5869.

17 I. Sun, J. R. Sanders and C. L. Hussey, *J. Electrochem. Soc.*, 1989, **136**, 1415–1419.

18 R. T. Carlin, R. A. Osteryoung, J. S. Wilkes and J. Rovang, *Inorg. Chem.*, 1990, **29**, 3003–3009.

19 G. Haarberg, W. Rolland, Å. Sterten and J. Thonstad, *J. Appl. Electrochem.*, 1993, **23**, 217–224.

20 G. R. Stafford and T. P. Moffat, *J. Electrochem. Soc.*, 1995, **142**, 3288–3296.

21 Y. Andriyko and G. E. Nauer, *Electrochim. Acta*, 2007, **53**, 957 – 962.

22 F. Endres, O. Hofft, N. Borisenko, L. H. Gasparotto, A. Prowald, R. Al-Salman, T. Carstens, R. Atkin, A. Bund and S. Zein El Abedin, *Phys. Chem. Chem. Phys.*, 2010, **12**, 1724–1732.

23 K. D. Childs, B. A. Carlson, L. LaVanier, J. F. Moulder, D. F. Paul, W. F. Stickle and D. G. Watson, *Handbook of Auger electron spectroscopy*, Physical Electronics, 1995.

24 W. Kantlehner, E. Haug, W. W. Mergen, P. Speh, T. Maier, J. J. Kapassakalidis, H.-J. Bräuner and H. Hagen, *Liebigs Ann. Chem.*, 1984, **1984**, 108–126.

25 M. Gnahm, C. Berger, M. Arkhipova, H. Kunkel, T. Pajkossy, G. Maas and D. M. Kolb, *Phys. Chem. Chem. Phys.*, 2012, **14**, 10647–10652.